Phase formation in Zr–Fe multilayers: Effect of irradiation

A. T. Motta
The Pennsylvania State University, Department of Mechanical and Nuclear Engineering, University Park, Pennsylvania 16802

A. Paesano Jr.
Instituto de Fisica, Universidade Estadual de Maringá, Paraná, Brasil

R. C. Birtcher
Materials Science Division, Argonne National Laboratory, Argonne, Illinois 60403

M. E. Brückmann, S. R. Teixeira, and L. Amaral
Instituto de Fisica, Universidade Federal do Rio Grande do Sul, Porto Alegre, Rio Grande do Sul, Brasil

(Received 30 September 1998; accepted for publication 4 February 1999)

We have conducted a detailed *in situ* study of phase formation in Zr–Fe metallic multilayers using irradiation and thermal annealing. Metallic multilayers with near equiatomic and Fe-rich overall compositions and with repetition thicknesses ranging from 7.4 to 33 nm were either irradiated with 300 keV Kr ions at various temperatures (from 17 to 623 K) or thermally annealed at 773 K while being observed *in situ*. The kinetics of multilayer reaction were monitored by following the diffraction patterns. For near equiatomic samples, irradiation causes complete amorphization. The dose to amorphization increases in proportion to the square of the wavelength, indicating a process controlled by atomic transport. Amorphization was also achieved by 900 keV electron irradiation at 25 K showing that displacement cascades are not required. The critical dose to amorphization was independent of temperature below room temperature and decreased above room temperature. The activation energy for this second process is 0.17 eV. For the temperature range studied, diffraction from Zr disappears first, indicating that amorphization takes place in the Zr layer by atomic transport of Fe from the Fe layers. These results are consistent with a combination of simple ballistic mixing at low temperature and either simple diffusion or radiation-enhanced diffusion at higher temperatures. Thermal annealing of the equiatomic samples at 773 K produced the same reaction products with slower kinetics. Ion irradiation of Fe-rich samples did not cause complete amorphization and intermetallic compounds Zr_3Fe and $ZrFe_2$ were observed in longer wavelength samples. Amorphization of Fe-rich samples was more sluggish, likely because there was competition with formation of other phases. The reaction kinetics were not proportional to square of wavelength for Fe-rich samples, indicating a process that depends on more than atomic transport. Thermal annealing at 773 K of a long wavelength, 57% Fe sample resulted in intermetallic compounds Zr_3Fe and $ZrFe_2$ which amorphized during subsequent irradiation. The ease of amorphization of equiatomic samples relative to Fe-rich samples can be explained by a narrower, single minimum free energy curve for the amorphous phase. © *1999 American Institute of Physics.*
[S0021-8979(99)01610-2]

I. INTRODUCTION

Phase formation in metallic multilayers by both solid-state reaction and ion irradiation has received considerable attention in recent years.[1–5] Metallic multilayers represent a model system to study the kinetics and thermodynamics of phase formation because they can be manufactured at given thicknesses and compositions, and be subjected to thermal annealing or irradiation under precisely controlled conditions. The Zr–Fe system is of particular interest because it can serve as a model system for the solid-state reaction between the late and early transition metals, and because the presence of Fe allows the use of hyperfine and magnetic techniques to complement structural x-ray diffraction techniques in detecting the appearance of new phases. It is also a system which has technological importance.[6–8]

Paesano, Teixeira, and Amaral[5] used Mössbauer spectroscopy to show that the final products of solid-state reaction depend on the overall multilayer composition. They found complete amorphization at the equiatomic composition after annealing at 773 K. In the Fe-rich and Zr-rich samples different combinations of intermetallic compounds, amorphous phases and pure Fe in the Fe-rich and Zr-rich cases were observed. Other researchers have found phase separation in the amorphous phase, as well as a dependence of the final products on modulation wavelength and overall composition.[5,9] However no systematic study of the influence of these parameters, and no detailed study of the kinetics of the reaction processes under irradiation have been reported.

The aim of this study is to conduct a systematic investigation of the influence of modulation wavelength λ (the thickness of one zirconium and one iron layer) and overall

TABLE I. Zr–Fe multilayers examined and experimental conditions.

Group	Sample designation	Thickness (nm)	Wavelength λ (nm)	Zr thickness (nm)	Composition (at. % Fe)	Irradiation temperature (K)
	10X	105	10.5	7	50	25, 293, 373, 473, 573, 623
50–58% Fe	7X	91	13	7.8	55	17, 293, 373, 473, 573
near	6X	90	15	10	50	Thermal anneal only
equiatomic	5XA	125	25	15.5	55	293
	5XB	95	19	10.8	58	Thermal anneal only
	4X	108	27	18	50	293, 373, 473, 573
64% Fe	13X	96	7.4	4	64	293, 373, 573
Fe rich	3X	100	33.3	18	64	17, 293, 373, 473, 573

composition (the nominal amount of iron and zirconium atoms in the ensemble of the multilayer) on phase formation in Zr–Fe multilayers under irradiation and thermal annealing. We have used *in situ* irradiation and annealing in a transmission electron microscope to directly measure the reaction kinetics and final reaction products for precisely defined conditions. In this study we expand on the previous work of the solid-state reaction results under thermal conditions obtained by Paesano, Teixeira, and Amaral, and investigate the effects of irradiation on the solid-state reaction process. We discuss the results in terms of previous work and of the existing models for solid-state reaction and irradiation mixing.

II. EXPERIMENTAL METHODS

Metallic multilayers of Zr and Fe were prepared by vapor deposition onto both a NaCl substrate [samples for transmission electron microscope (TEM)], and onto oxidized Si wafers (for the other characterization techniques) in a Balzers UMS 500P dual gun system at a base pressure of 5×10^{-9} Torr at room temperature. The total sample thickness was kept around 100 nm to make the multilayers electron-transparent at 300 keV. Both the modulation wavelength λ and the overall composition were varied, as shown in Table I. Irradiated samples were also subjected to thermal annealing. The sample designation refers to the number of wavelength repetitions in the sample and will be used throughout this work to identify the samples.

The samples were characterized with Rutherford backscattering spectroscopy (RBS) and Mossbauer spectroscopy (CEMS) at the Institute of Physics of the Federal University of Rio Grande do Sul, in Porto Alegre, Brazil. The RBS analyses were performed using an alpha particle beam of 760 keV with incident scattering angles of 0° and 175°. The overall resolution of the RBS spectrometer was 13 keV. The RBS spectrum of the 5XA multilayer, Fig. 1, shows that the nominal wavelength was closely reproduced in the deposited film and that the interfaces are sharply defined. Similar characterization was performed for all samples.

Samples for TEM were prepared by floating the multilayers on de-ionized water onto Cu grids. They were examined in the intermediate voltage transmission electron microscope (IVEM) at Argonne National Laboratory. This is a Hitachi 9000, microscope operated at 300 keV with an attachment that permits *in situ* ion irradiation of the sample.[10] The irradiation temperature can be controlled from 15 to 973 K, with a precision of 1–2 K. Ion and electron irradiations at 25 K were conducted in the Kratos high voltage electron microscope operated at 900 keV at the Center for Electron Microscopy at Argonne. *In situ* thermal annealing experiments were conducted in a heating stage at 773 K.

TEM examinations showed that the as-deposited layers were polycrystalline body-centered-cubic (bcc)-Fe and hexagonal-close-packed (hcp)-Zr, for all compositions and wavelengths. The grains in the Fe layers were randomly oriented, while the Zr layers showed a preferentially basal texture, as evidenced by the absence of the (0002) reflection from the diffraction pattern. For the sample with the smallest Zr wavelength (13×, $\lambda=4$ nm) the Zr lines were diffuse, so that the $10\bar{1}1$ and $10\bar{1}0$ lines could not be separated. This observation is in agreement with those of Vlassak and co-workers[11] who observed that below a wavelength of 4 nm, Fe/Zr multilayers became amorphous, and that just above 4 nm, multilayers had amorphous interfaces.

Irradiations were conducted with 300 keV Kr ions at temperatures from 25 to 623 K, at an ion current of approximately $1.87\times10^{12}\,\mathrm{cm^{-2}\,s^{-1}}$ to doses as high as 2×10^{16} $\mathrm{cm^{-2}}$. During *in situ* irradiation or annealing, the electron diffraction patterns were systematically recorded. Bright-field and dark-field micrographs were also taken. Phase identification was made from diffraction rings measured from the negatives. The camera length variations of about 1% be-

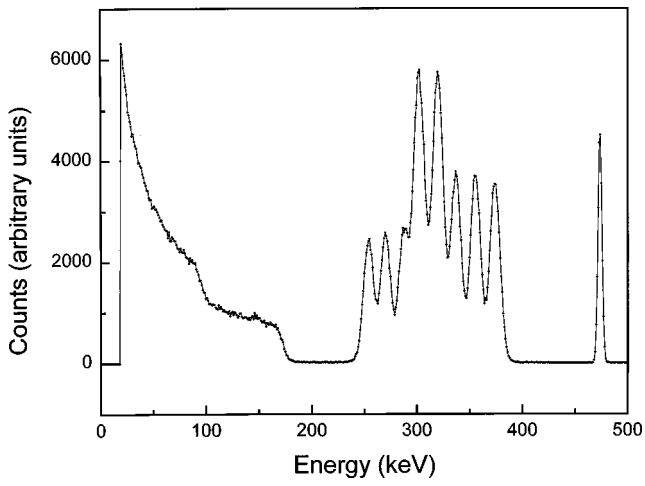

FIG. 1. RBS profile of as-deposited Zr–Fe metallic multilayers. The one shown is 5XA (15.5 nm Zr and 9.5 nm Fe).

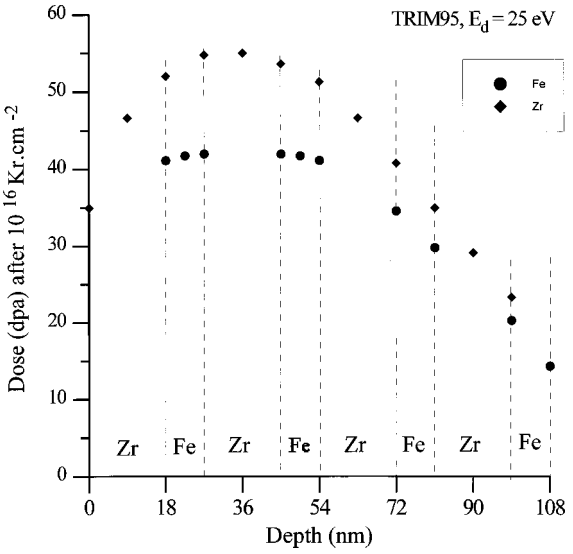

FIG. 2. Displacements per atom after 10^{16} Kr ion cm^{-2}, calculated for the 4X multilayer ($\lambda = 10.8$ nm) using the TRIM code. A displacement energy of 25 eV was assumed for both layers.

tween exposures were corrected by normalizing all measurements to the Fe (110) spacing at 0.202 nm. Vacuum in the microscope was about 2×10^{-7} Torr.

Figure 2 shows a transport of ions in matter (TRIM)[12] simulation of the number of displacements caused by the Kr ion beam assuming a displacement energy of 25 eV, for the 4X multilayer. At this energy, most ions are stopped within the sample. The displacement rate changes as the ion loses energy so that the individual multilayers are irradiated at different rates. Ion fluxes were between 1.25×10^{12} to 5×10^{12} ion.cm^{-2} s^{-1}. For the most frequently used flux of 1.87×10^{12} ion.cm^{-2} s^{-1}, the displacement rate in the sample ranged from 10^{-2} to 5×10^{-3} dpa/s in the Zr layers and from 8×10^{-3} to 2×10^{-3} dpa/s in the Fe layers.

After long exposures at high temperature, we detected rings indexed as monoclinic ZrO_2. No oxide was observed either during thermal annealing without irradiation or during irradiation at low temperature. For the equiatomic samples, in the absence of oxidation, no Fe is left over, i.e., in the absence of ZrO_2 formation, all Fe eventually reacts with Zr. Samples with a half layer of Fe on top and bottom to protect the Zr layers from exposure and oxidation proceeded to complete amorphization without oxide formation.

III. RESULTS

A. Kr ion irradiation

Ion irradiation causes new phases to form because of the reaction of the Zr and Fe multilayers. Some amount of amorphous phase was formed in all samples studied; the amorphous phase formed homogeneously in the plane of the layers (i.e., no variation in amorphous phase content with position in the observation plane of the sample). Amorphous phase formation was accompanied in some cases by the for-

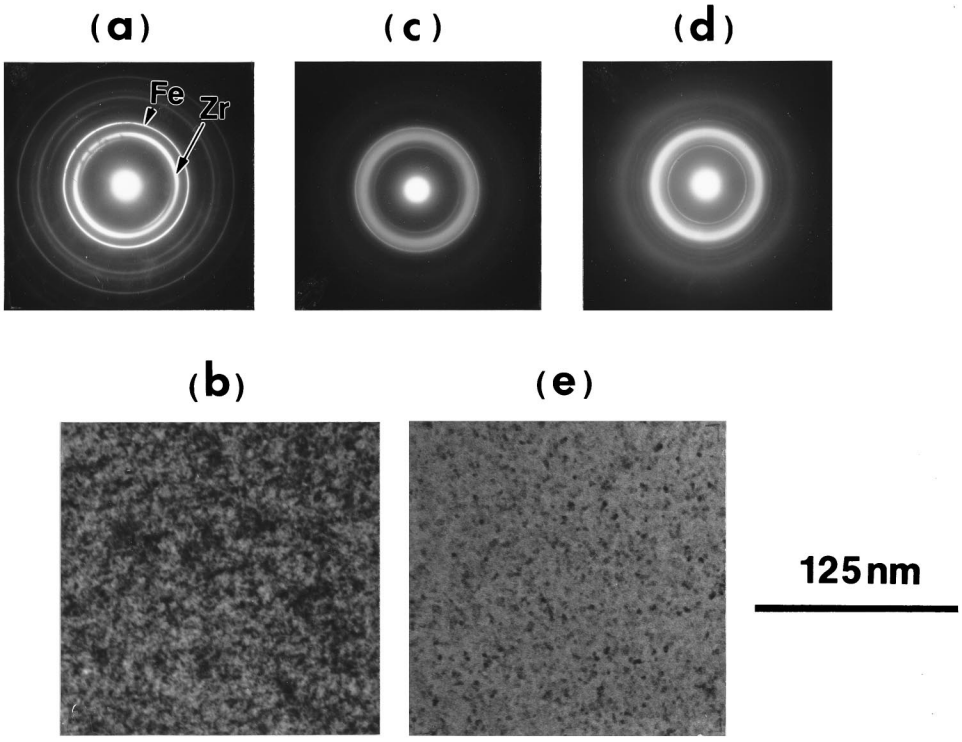

FIG. 3. Bright-field micrographs and diffraction patterns showing a typical reaction sequence for the amorphization of a 10X Zr–Fe multilayer, irradiated with 300 keV Kr ions at 473 K, while observed *in situ* in the microscope. (a) Diffraction pattern of as-deposited sample showing hcp-Zr and bcc-Fe, (b) bright-field micrograph showing as-deposited sample, (c) diffraction pattern of sample after irradiation to 2.5×10^{14} cm^{-2} showing that an amorphous phase has formed, the Zr lines have disappeared and the Fe lines have become weaker, (d) after irradiation to 10^{15} cm^{-2}, the intensity of the amorphous phase has increased considerably, while the intensity of the Fe line has been reduced nearly to zero; an oxide line (ZrO_2) is also visible, and (e) bright-field micrograph showing the change in contrast associated with amorphization.

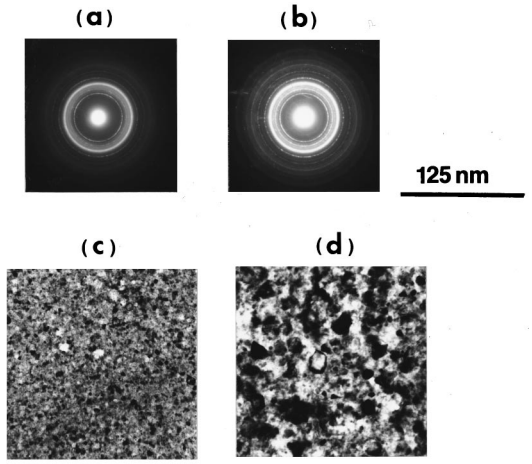

FIG. 4. Bright-field micrographs and diffraction patterns showing a typical *in situ* recrystallization sequence: (a)(b) diffraction patterns after post-irradiation annealing for 1200 and 1500 s at 973 K, showing that recrystallization has taken place, with the formation of crystalline intermetallic compounds (c)(d) corresponding bright-field micrographs after 20 and 25 minutes of annealing, showing the change in contrast associated with the growth of grains of crystallinr intermetallic compounds.

mation of intermetallic compounds. Ding, Okamoto, and Rehn, also observed homogeneous amorphization during ion induced amorphization of Zr–Ni bilayers, but saw heterogeneous phase formation in Zr–Au bilayers.[13] The final products and the reaction kinetics depend both on the wavelength and on the overall composition of the multilayers. Samples either become completely amorphous or approach a steady state containing a mixture of unreacted Fe and amorphous phase. In the remainder of the article we refer to the dose to either complete amorphization or to the steady state earlier described, as the dose to amorphization. To facilitate the discussion we group the results by overall multilayer composition.

1. Near-equiatomic samples (Fe concentration between 50 and 58 at. %)

Three wavelengths were studied: 4X, 10X, and 7X. For all these samples, as the fluence increases, the Zr and Fe rings weaken and a broad halo associated with the Zr–Fe amorphous phase appears and becomes more intense. At steady state the near equiatomic samples contained mostly amorphous Zr–Fe and some remnant bcc-Fe.

Figures 3(a) to 3(e) show a typical irradiation performed on a 10X multilayer. Initially the as-deposited multilayers exhibit diffraction rings indexed as hcp-Zr and bcc-Fe. As the irradiation proceeds, the Zr rings weaken and disappear, and a diffuse amorphous ring appears. This amorphous ring becomes stronger with further irradiation and the Fe rings become progressively weaker. In the final steady state, there is a strong component of the amorphous phase and a small amount of localized remanent Fe (possibly connected to oxide formation, as mentioned earlier). *In situ* recrystallization performed at 700 K for 20–25 min produces the intermetallic compounds $ZrFe_2$ and Zr_3Fe as shown in Figs. 4(a) to 4(d).

Figure 5(a) is the diffraction pattern of the as-deposited multilayer indicating the presence of bcc-Fe and hcp-Zr. Dark field micrographs taken from the Zr rings [Fig. 5(b)] and from the Fe rings [Fig. 5(c)] illuminate the respective sets of grains. In the as-deposited state both metallic multilayers exhibit a grain size of 10–15 nm as also seen in the bright-field micrograph Fig. 5(d). After irradiation to $5\times10^{15}\,\mathrm{cm}^{-2}$ at 17 K, the Zr grains disappear from the dark-field image, while the Fe grains increase in size [Figs. 5(f)

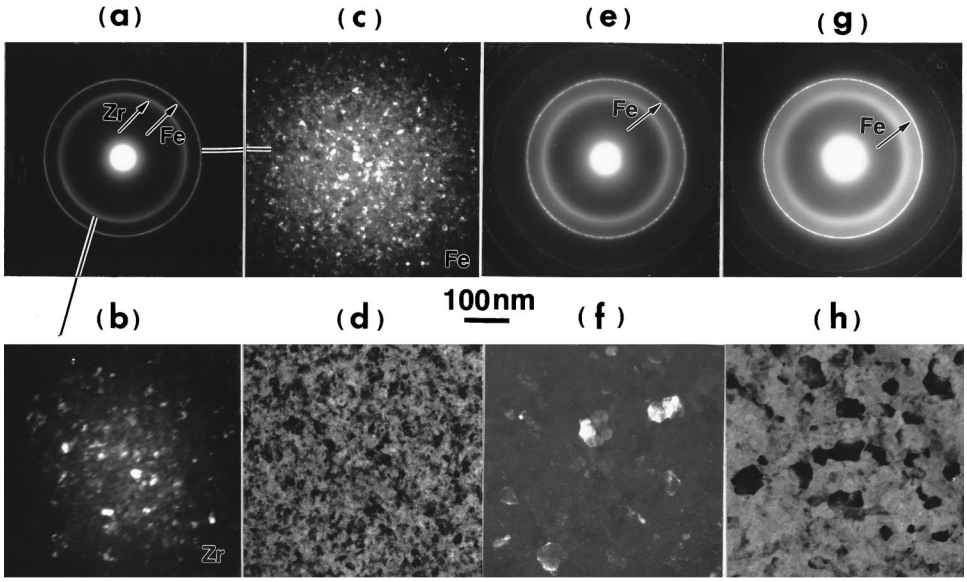

FIG. 5. Grain growth during Kr ion irradiation of 3X Zr–Fe multilayer at 17 K. (a) Diffraction pattern of as-deposited multilayer showing bcc-Fe and hcp-Zr lines; dark fields taken using the Zr reflection, (b) using the Fe reflection; (c) as indicated, to show the starting grain size in each of the layers; (d) bright field of the as-deposited multilayer; (e) diffraction pattern after irradiation to $2\times10^{15}\,\mathrm{cm}^{-2}$ showing that the Zr line has disappeared, that an amorphous halo has formed and that the Fe line has become more ''granular'' indicating grain growth; (f) dark field taken using the Fe line, showing that the Fe grains have grown considerably; (g) diffraction pattern taken after irradiation to $5\times10^{15}\,\mathrm{cm}^{-2}$; and (h) corresponding bright field showing that grain growth has saturated. (Bright-field and dark field magnification is about 33,000X).

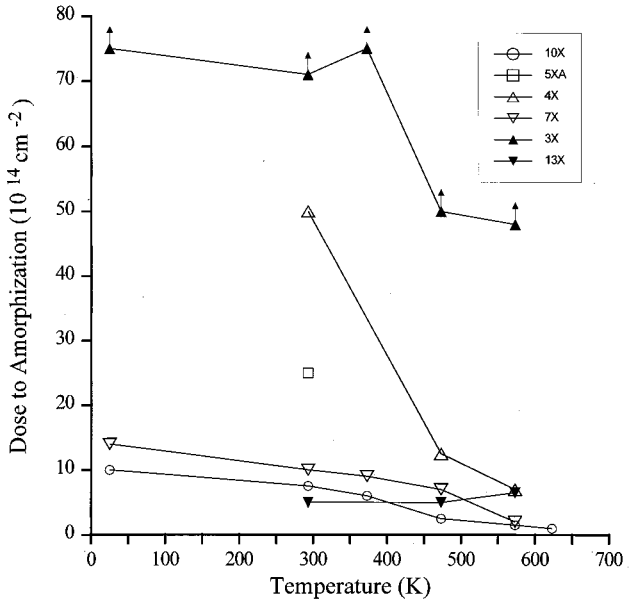

FIG. 6. Dose to amorphization as a function of irradiation temperature for 300 keV Kr ion irradiation of several Zr–Fe multilayers. The upward pointing arrows for the dose to amorphization measured in the 3X multilayers indicate that full amorphization was not achieved for these samples.

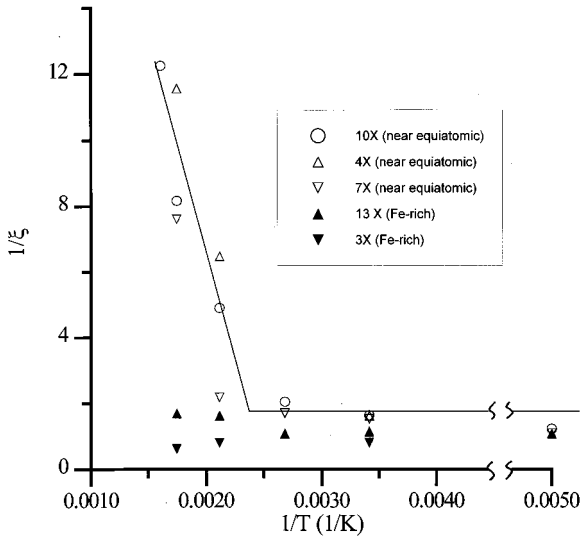

FIG. 7. The square of the multilayer wavelength divided by the dose to amorphization ($1/\xi$) in units of $10^{-14}\,\mathrm{nm^2\,ion^{-1}\,cm^2}$ and plotted against inverse temperature in a logarithmic scale, for the amorphization of several Zr–Fe multilayers under 300 keV Kr ion irradiation. Note change of scale. The results for equiatomic multilayers show an athermal regime then a thermal regime, controlled by atomic transport. The Fe-rich multilayers do not follow the same behavior.

and 5(h)], similar to the observations of Karpe *et al.* at room temperature.[3] These observations of grain growth will be reported in greater detail elsewhere.[14]

Amorphization occurs at temperatures from 17 to 623 K. Since the displacement rate is not homogeneous over the thickness of the sample (as shown in Fig. 2), the multilayer reaction occurs at different times for different depths in the sample, causing some temporal spread in the observed dose to amorphization. The dose to amorphization decreases as the temperature increases, likely due to a combination of faster solid-state reaction and ion beam mixing, as shown in Fig. 6. As the wavelength increases, the dose to amorphization increases in proportion to the square of the wavelength thickness. Figure 7 shows the square of the Zr half thickness divided by the dose to amorphization [this is the inverse of the parameter ξ defined in Eq. (8) later] against the inverse of temperature. The half thickness of the Zr layer has been chosen because, as discussed later, the mobile species is Fe and the reaction consumes the Zr layer. The data from the different types of irradiation (different wavelengths, composition varying from 50% to 58%) are all on the same line, indicating that the dose is proportional to the square of the wavelength. It is also apparent from Fig. 7 that there are two temperature regimes. The thermal regime starts slightly above room temperature and has an activation energy of 0.17 eV.

2. Fe-rich samples (64 at.% Fe)

The effect of overall composition on the phase formation kinetics was studied by samples with 64 at.% Fe: one (3X) with the same Zr-layer thickness (18 nm) as the 4X equiatomic sample and second with very small wavelength (13X), to be compared with the 10X equiatomic sample. In both samples, the increased Fe content significantly increased the dose to amorphization (or in this case the dose to steady state). As shown in Fig. 6, although the overall trends are similar, (i.e., the dose to amorphization decreases with increasing irradiation temperature) amorphous phase formation was significantly more sluggish in the Fe-rich samples. This is indicated in Fig. 6 by the upward pointing arrows in the large wavelength sample, which did not reach steady state for the irradiation time used.

The shorter wavelength Fe-rich sample (13X) was irradiated at 293, 373, and 573 K. The phases formed are qualitatively similar to those formed during irradiation of the commensurate equiatomic sample multilayer (10X): only an amorphous phase was observed, (along with remanent Fe) and no intermetallic compounds formed at any temperature to doses up to $1.5\times10^{16}\,\mathrm{cm^{-2}}$. However, the doses necessary for the amorphization reaction were higher than in the 10X sample by factors of 2–4.

The longer wavelength samples did not achieve steady state after a fluence of $1.5\times10^{16}\,\mathrm{cm^{-2}}$. This is why the points for 3X are shown with an upward pointing arrow indicating that full reaction occurs at higher fluences. The reaction products were also different than in the case for near-equiatomic samples. In particular, the amount of Fe left over after the transformation was higher than in the case for near-equiatomic samples. This could be due to different phase equilibria in the Fe-rich samples or to different kinetics prevailing at the different compositions, as will be discussed later.

The Fe-rich sample (3X) was irradiated at 17, 293, 373, 473, and 573 K. At all temperatures, some amorphous phase formation was observed, and in no case was the Fe completely consumed. However, different final products were obtained depending on the temperature. At the two highest

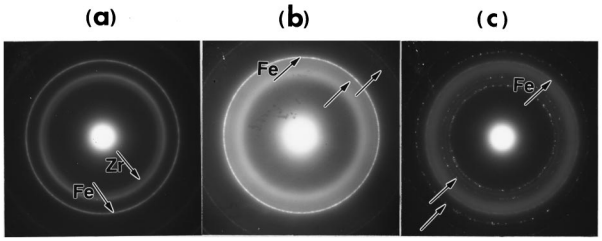

FIG. 8. Diffraction patterns showing the reaction products obtained at steady state for the 300 keV Kr ion irradiation of the 3X multilayer, (a) as-deposited multilayer, (b) after irradiation to $5\times10^{15}\,\mathrm{cm}^{-2}$ at 17 K; arrows show diffraction lines corresponding to the intermetallic compound $ZrFe_2$, and (c) after irradiation to $1.5\times10^{16}\,\mathrm{cm}^{-2}$ at 473 K; arrows show diffraction lines corresponding to the intermetallic compound Zr_3Fe.

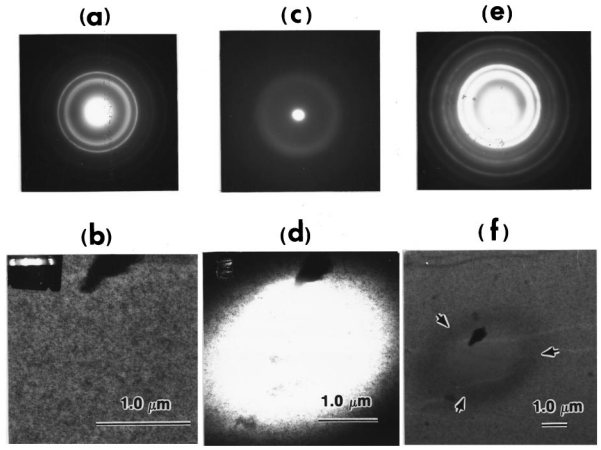

FIG. 9. Amorphization of 10X Zr–Fe multilayer sample under 900 keV electron irradiation performed at 25 K. (a) Diffraction pattern taken before irradiation showing only the crystalline rings; (b) bright-field micrograph showing the unirradiated area; (c) diffraction pattern taken after irradiation showing an amorphous halo; (d) short exposure bright field showing the size of the condensed electron beam during irradiation; (e) diffraction pattern taken after irradiation from region not under the beam, showing only crystalline rings; and (f) bright-field micrograph showing amorphous region after 64 min of irradiation (4 dpa).

temperatures (473 and 573 K), diffraction lines corresponding to the intermetallic compound Zr_3Fe were observed at fluences of approximately $5\times10^{15}\,\mathrm{cm}^{-2}$. At the two intermediate temperatures (293 and 373 K), no crystalline intermetallic compound diffraction lines appeared during irradiation. At the lowest temperature (17 K) diffraction lines corresponding to another intermetallic compound ($ZrFe_2$) appeared at $5\times10^{15}\,\mathrm{cm}^{-2}$. Figure 8 shows the diffraction patterns obtained at the end of the irradiation time for the longer wavelength Fe-rich samples (3X). Figure 8(a) shows the diffraction pattern for the as-deposited multilayers, Fig. 8(b) shows the diffraction pattern obtained after irradiation to $5\times10^{15}\,\mathrm{ion.\,cm}^{-2}$ at 17 K with arrows indicating the lines corresponding to $ZrFe_2$ and Fig. 8(c) shows the pattern obtained after irradiation to $1.5\times10^{16}\,\mathrm{ion.\,cm}^{-2}$ at 473 K, where arrows indicate the lines corresponding to Zr_3Fe.

B. Electron irradiation induced amorphization

The role of displacement cascades in phase formation in Zr–Fe multilayers was investigated by irradiating the near-equiatomic 10X multilayer sample with 900 keV electrons at room temperature at a dose rate of $10^{-3}\,\mathrm{dpa\,s}^{-1}$. Room temperature electron irradiation alone can cause amorphization of this multilayer sample. Figures 9(a) and 9(b), show the 10X multilayer, before the start of irradiation with the corresponding diffraction pattern; in Fig. 9(d) the beam is focused to provide the high electron flux necessary for amorphization. Figure 9(c) shows the diffraction pattern obtained after irradiation to a dose of 4.4 dpa, showing a diffuse halo and no crystalline rings. At this dose, an amorphous region is visible in Fig. 9(f) as the region of low contrast. The beam heating at this electron flux is estimated to be around 10–20 K, and the whole experiment takes approximately 2 h so it is unlikely that amorphization is a thermally driven effect in this case, especially since other regions of the sample (not under the beam) show no effect, as shown in the diffraction pattern taken from one of these regions after amorphization is finished [Fig. 9(e)]. This result demonstrates that irradiation amorphization in multilayers can be achieved in the absence of displacement cascades. Amorphization of layered metallic materials by electron irradiation has also been observed by Lin, Seidman, and Okamoto,[15] who amorphized Ge–Al and Si–Al bilayers with a 1 MeV electron beam. They found that a recoil-implantation model explained well their results.

C. Thermal annealing

Thermal annealing at 773 K was performed for all the multilayers studied. As in the case of ion irradiation, the final reaction products depend on both the wavelength and the composition of the multilayer. The 10X, 6X, and 4X multilayers all reach the same steady state of only an amorphous halo and residual Zr and Fe (with no traces of zirconium oxide), as shown in Fig. 9 for the 6X and 4X multilayers and in Fig. 3 for the 10X multilayer. The amount of amorphous phase formed, (estimated by the relative intensities of the amorphous and crystalline rings), appears to be less than in the ion irradiation case, and the final mixture of phases contains remnants of both metals.

However, for the samples containing intermediate (55–58% at) Fe concentrations there was a marked difference in behavior with wavelength. Intermetallic compounds $ZrFe_2$ and Zr_3Fe form in the longer wavelength sample (5XA 25 nm) (as shown in Fig. 10). These intermetallic compounds have the standard structures of the orthorhombic Zr_3Fe and cubic $ZrFe_2$.[16] The intermetallic compounds were already present at the end of the temperature ramp ($1.6\,\mathrm{K\,s}^{-1}$), and do not change significantly afterwards. Irradiation of these intermetallic compounds causes them to become amorphous. Only an amorphous phase was observed in films with shorter wavelength (5XB-13 nm) and (7X-19 nm), even after long annealings of up to 2 h at 773 K, although a few hints of intermetallic compound formation appeared at the end of annealing of 7X, as shown in Fig. 10.

During thermal annealing of the two 64% Fe rich composition films, the short wavelength film (13X) quickly arrived at similar reaction products as did the equiatomic films,

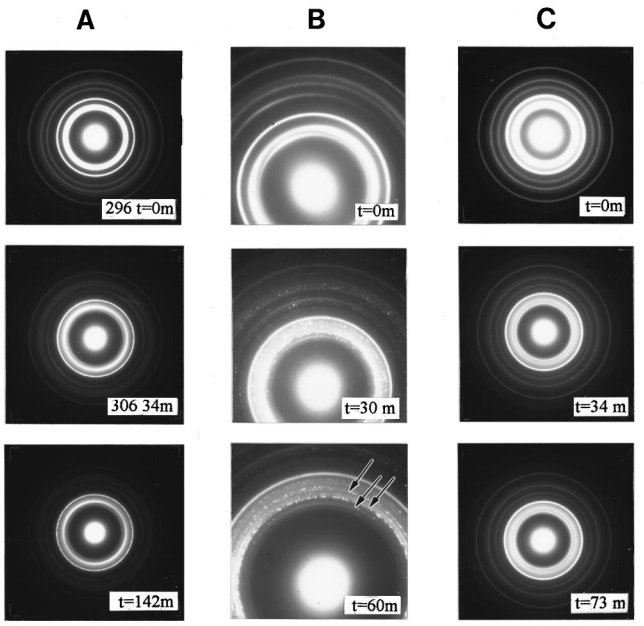

FIG. 10. Diffraction pattern sequences taken from Zr–Fe multilayers showing the reaction products obtained after thermal annealing at 773 K for the times indicated: (a) 6X multilayer (near equiatomic, $\lambda=15$ nm, Zr thickness 10 nm): only an amorphous phase and faint Fe rings remain after annealing for 73 min; (b) 5XA multilayer (55% at Fe, $\lambda=25$, Zr thickness 15.5 nm): both an amorphous phase, and new crystalline intermetallic compounds form. The arrows show the diffraction lines corresponding to the intermetallic compounds $ZrFe_2$ and Zr_3Fe. These form very quickly (at the end of temperature ramp, or at $t=2$ m); (c) 7X multilayer; (55% at Fe, $\lambda=13$, Zr thickness 7.8 nm): an amorphous halo and the original pure element diffraction lines dominate; only very faint signs of crystalline intermetallic compounds appear after a long annealing.

i.e., amorphous phase and Fe. The longer wavelength sample (3X) showed very little reaction for the annealing times used.

D. Summary of experimental results

The summary of the reaction products formed under different conditions is shown in Table II. Intermetallic compounds tend to form more easily in large wavelength, Fe-rich samples. Ion irradiation is more efficient than thermal annealing at forming the amorphous phase and the transformation is more sluggish in Fe-rich samples.

IV. DISCUSSION

To discuss the earlier results, it is necessary to place them in the broader context of previous work in phase formation in Zr–Fe multilayers. In this section, we briefly review previous work in this area.

A. Solid-state reaction in Zr–Fe multilayers

Clemens and Suchowski[17] first used this system to demonstrate the occurrence of the solid-state reaction in iron-based metallic multilayers. Several researchers have studied the effect of irradiation and thermal annealing on phase formation in Zr/Fe multilayers,[3–5,8,9,17–35] using CEMS,[5] calorimetry,[34] magnetization,[4] x-ray, resisitivity, RBS, mechanical properties,[11] or TEM.[19] Kiauka and Keune[9] found that the maximum Fe thickness that reacts by solid-state reaction is 2 nm. Films thicker than 2 nm saturate and do not evolve even after 100 h at 660 K. This observation indicates that there is a maximum thickness of 2 nm for complete amorphization. However Paesano, Teixeira, and Amaral achieved full amorphization of equiatomic ZrFe layers with large wavelengths ($\lambda=15$ nm) using CEMS after annealing at 773 K for 3 h[31] and Yamamoto and co-workers achieved complete amorphization of an equiatomic alloy with $\lambda=18$ nm after 2 h annealing at 773 K.[8] Also Michaelsen, Piepenbring, and Krebs[36] saw complete amorphization of ZrFe multilayers after solid state reaction. Geisler and co-workers found a critical thickness for the Fe layer of 2 nm[37] below which the magnetic and elastic properties of the Zr–Fe multilayer suffer a sudden transition. The authors attribute this to a crystal-to-glass transition that occurs below that thickness.

TABLE II. Summary of reaction products.

Sample number	Overall Fe content (at. %)	Kr ion irradiation (17–623 K)	Thermal annealing at 773 K
10X	50%	Amorphous	Amorphous +Zr+Fe
7X	55%	Amorphous	Amorphous + intermetallic compounds
6X	50%	···	Amorphous +Zr+Fe
5XA	55%	Amorphous	Intermetallic compounds ($ZrFe_2$, Zr_3Fe)+ amorphous
5XB	58%	···	Amorphous
4X	50%	Amorphous+Fe	Amorphous +Zr+Fe
13X	64%	Amorphous	Amorphous+Fe
3X	64%	Amorphous + intermetallic compounds ($ZrFe_2$ at low temperature, Zr_3Fe at high temperature)	Little reaction observed

In principle, any practical limit on the amount of reaction (or of amorphous phase formed) is governed by the metastable equilibrium between the amorphous phase and the crystalline solid solutions of one element in the other. A ''critical thickness'' of amorphous phase as proposed by Kiauka and Keune[9] would be not only dependent on kinetics, but also on sample composition. Thus, it is likely that the critical thickness observed by Kiauka and Keune is actually a practical limit related to kinetic factors specific to their samples and experiment.

Other researchers[22,30] have demonstrated the importance of grain boundaries in amorphization of Zr–Fe multilayers under solid-state reaction. Little amorphization between a deposited Fe layer and a Zr substrate was observed when they switched from polycrystalline Zr substrate to single crystal Zr substrate. The authors postulated that the reaction occurs preferentially along the grain boundaries of Zr. This was supported by the work of Otto and co-workers[30] who

found a mixture of grain boundary and volume diffusion with activation energies of 0.35 and 0.93 eV, respectively.

Krebs and co-workers[4,26,27] used magnetization of equiatomic multilayers after solid-state reaction to determine that the critical temperature for the fully reacted multilayers was 75 K for an amorphous phase containing 60% Fe.[38] They infer that there is another (nonmagnetic) amorphous phase containing about 35% Fe, and that the final reaction products are a mixture of two amorphous phases of different compositions. This observation is supported by chemical diffusion experiments of Karpe *et al.*[20] who noticed that an amorphous Zr–Fe layer loses or gains Fe depending on the overall multilayer composition in accordance with a double minima free energy curve. Kopcewicz *et al.*[24] studied the quadrupole splitting distribution P(QS) in amorphous Zr–Fe alloys formed by ion irradiation and found that the P(QS) for equiatomic amorphous alloys showed distinct features which indicate the presence of two different amorphous phase compositions. These observations were explained[4] by a model for the free energy curve of amorphous Zr–Fe which contains two minima near the compositions 33% and 66% Fe. Since there is evidence that the chemical short-range order in the amorphous is similar to that found in the intermetallic compounds Zr_2Fe and $ZrFe_2$,[39] this would provide a natural explanation for the greater stability of the amorphous phase at those compositions.

However, additional measurements of isomer shifts[40] are consistent with the presence of only one amorphous phase with composition 50% that forms after annealing samples of various wavelengths at 623 K for times ranging from 15 min to 24 h. These results are in direct contrast to those obtained by Kopcewicz and co-workers,[24] and there is no readily available explanation for the difference.

Ding, Okamoto, and Rehn[19] studied the Zr–Fe system, using RBS to detect the amount of mixing as a function of fluence and temperature. They detected two regimes, characterized by two activation energies of 0.07 and 1.4 eV (above 500 K). Their study, however, could not discern between the different phases formed, and was performed for a single wavelength and composition. Kopcewicz and Williamson[18] studied amorphization of Zr–Fe multilayer using ion beams detecting the transformation by CEMS. They found that the amorphous fraction was proportional to the dose$^{1/2}$ (consistent with a transport-controlled reaction mechanism). Recently investigations of amorphization of Zr/Fe multilayers with swift heavy ions indicated a two-step mixing process, where initially mixing occurs by Fe diffusion and later by amorphization along ion tracks.[41]

B. Driving force for amorphization

Both thermal annealing and ion irradiation can cause the formation of new phases in Zr–Fe multilayers. This process is energetically favorable, as there is a net reduction of free energy when we transform separated constituents (present in the as-deposited multilayers) to a crystalline intermetallic compound or to an amorphous compound that is mixed at the atomic level. Whether the compound formed is amorphous or crystalline depends on the mixing dynamics and on the stability of an amorphous solid at the overall composition.

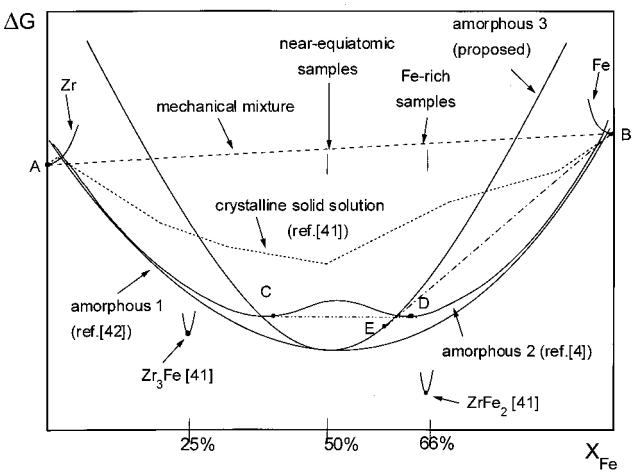

FIG. 11. Schematic free energy curves for the various stable and metastable phases in the Zr–Fe binary system. The stable phases at the temperatures of interest are hcp-Zr, Zr_3Fe, $ZrFe_2$, and bcc-Fe. Also shown are three possible alternatives for the metastable amorphous phase, as well as the mechanical mixture and the crystalline solid solution. See text for discussion.

Figure 11 shows a proposed free energy diagram for the Zr–Fe system for a fixed temperature that can help explain some of the results above. The thermodynamically stable phases are the two pure metal solid solutions (bcc-Fe and hcp-Zr) and two crystalline intermetallic compounds ($ZrFe_2$ and Zr_3Fe). At the start of the experiments, the as-deposited metallic multilayers are located on the line $A-B$ which represents the mechanical mixture of Zr and Fe (the exact spot depends on the overall composition). Once the multilayer reaction starts the system forms a combination of the metastable and stable compounds depending on which compounds are kinetically available. Rodriguez *et al.* calculated the free energy curve for the crystalline solid solution shown in Fig. 11.[42] As mentioned earlier, Krebs, Webb, and Marshall[4] propose a free energy curve for the amorphous phase containing two minima (such as the schematic amorphous 2 curve shown in Fig. 11). Bruckmann *et al.*[43] calculated the amorphous Zr–Fe free energy curve by modeling the amorphous phase as a regular solution model (amorphous 1). Starting from the mechanical mixture, the formation of the amorphous phase provides a greater degree of free energy reduction than the formation of a crystalline solid solution, and thus one would expect to observe it as the preferred metastable phase.

Our results show that complete amorphization is easier for equiatomic samples than for Fe-rich samples, under ion irradiation or thermal annealing. These results are in agreement with the results of Kiauka who observed a mixture of Fe and amorphous phase after thermal annealing at 620 K for 5 h in 60 at. % Fe-40 at. % Zr samples[9] and 660 K for 118 h in 55 at. % Fe-45 at. % Zr.[22] The results are also in agreement with the results of Paesano, Teixeira, and Amaral,[5,31] who found much less amorphous phase formation in the 66 at. % Fe samples than in 50 at. % Fe samples.

Although the phase diagram only gives information about equilibrium phases, (and clearly the amorphous phase is metastable), it is possible to use phase diagrams to discern which metastable equilibria are likely. Both curves 1 and 2 for the amorphous phase shown in Fig. 11 predict complete amorphization near the equiatomic composition. Curve 2 predicts an equilibrium mixture of two amorphous phases at compositions *C* and *D*, while curve 1 predicts a single amorphous phase. Our experiments cannot distinguish between these two results. However, both curve 1 and curve 2 also predict complete amorphization at 66%. Thus these curves are not good indicators of phase stability under irradiation, because they are inconsistent with the observation that complete amorphization occurs only at 50%.

The actual range for the amorphous phase is not as broad as indicated by curve 1. The regular solution model assigns a free energy to the amorphous curve that is coincident with the pure metals at small concentrations, but this is physically unreasonable, since the amorphous phase does not form upon the addition of very small amounts of Fe to Zr. In other words, the free energy of the amorphous phase should rise more steeply with concentration than the regular solution model predicts. By assuming that the free energy of the amorphous phase is higher than the pure metal phases at small concentrations, we will obtain the hypothetical curve ''amorphous 3.'' This curve predicts that at 50% Fe we would see only the amorphous phase, and that at 66% Fe we would find an equilibrium between an amorphous phase of composition *E* and bcc-Fe (equilibrium $B-E$ in Fig. 11), as observed experimentally.

C. Kinetics of amorphization

The experimental results in Table II and Fig. 6 show that both the kinetics of phase formation and the final reaction products depend on both the overall composition and the multilayer wavelength. As the multilayer wavelength increases, it becomes more probable to find stable crystalline intermetallic compound phases as the product of solid state reaction processes. The ion dose for amorphization is proportional to the square of the wavelength. As the Fe concentration increases, the kinetics of phase formation become more sluggish, and it is also more probable to observe intermetallic compounds as the reaction products.

As mentioned earlier, in reacting metallic multilayers of elements with negative heat of mixing, amorphization *reduces* the overall free energy. This is in contrast with the amorphization of intermetallic compounds under irradiation, in which the stable intermetallic phase, present at the outset, is destabilized by damage accumulation, allowing the amorphous phase to appear.[44] A net free energy *increase* occurs in this case. Amorphization of thermodynamically stable intermetallic compounds thus requires the external input of energy (from irradiation or from processes such as ball milling). The transformation should in that case be properly classified as *irradiation-induced*. In the case of metallic multilayers under both thermal annealing and ion irradiation, the phases that appear depend on the kinetics by which the reduction of energy is achieved, so it is possible to have both *irradiation-enhanced* and *irradiation-induced* transformations.

This study was conducted to discern what experimental conditions (ion type, dose, dose rate, irradiation temperature, annealing time, and temperature) and multilayer characteristics (wavelength and composition) lead to one process or the other. Previous studies[31] have shown that there is little solid-state reaction in Zr–Fe multilayers after thermal annealing below 623 K. Thus, the multilayer amorphization observed in this study below room temperature is *caused* by irradiation. It is clear, however, that temperature also plays a role in effecting the transformation, since, above 293 K the dose to amorphization decreases with increasing temperature. We now discuss the amorphization mechanism in more detail.

D. Amorphization mechanism

Amorphization by mixing occurs when interdiffusion of the two elements in a multilayer causes the local concentration of the alloying element to increase to a level where the free energy difference between the solid solution and the amorphous compound provides enough driving force for the transformation to occur. For the amorphization reaction to take place at the interfaces of metallic multilayers, a critical concentration of the mobile element into the immobile element must be achieved. From the preceding considerations the condition for amorphization is

$$C(x) > C_{\text{crit}}. \tag{1}$$

Assuming that only one species is mobile (as indeed is the case for the Zr–Fe system), full amorphization of the immobile layer requires that Eq. (1) is satisfied at the midpoint of the layer. It is thus necessary to transport the mobile element across the phase interfaces, through the diffusion barrier, and to nucleate the new phase. We assume here, that nucleation and interfacial transport are relatively fast, and that achievement of this critical concentration is controlled by the rate of atomic transport.

Three main processes that can contribute to the atomic transport in multilayers:

(i) thermal diffusion;
(ii) irradiation enhanced thermal diffusion; and
(iii) athermal irradiation mixing (ballistic mixing).

The overall mixing during irradiation results from the combined action of these three processes and can be described by Fick's law, $J=-D(\partial C/\partial x)$, where J is the flux, D is the diffusion coefficient, and C is the concentration. We assume here that Fick's law is valid for ballistic processes as well, which may not be strictly true. Martin[45] performed a numerical evaluation of the validity of Fick's law in the presence of ballistic jumps, and found that if jumps occurred to the third nearest neighbor, Fick's law was found not to be valid for wavelengths smaller than 15 lattice parameters, which is certainly in the range of some of the diffusion processes considered here. While recognizing these limitations, we use the current assumption for simplicity, and we will show later that this assumption has some validity.

The difference between atomic transport caused by these different processes lies in their diffusion coefficients. Thermal diffusion is described by a diffusion coefficient of the form

$$D_{\text{th}} = C_{\text{def}} D_{\text{def}}, \tag{2}$$

where C_{def} is the concentration of the defect responsible for diffusion. The diffusion coefficient of this defect is

$$D_{\text{def}} = \frac{1}{6} a_0^2 \nu \exp(-E/kT), \tag{3}$$

where a_0 is the jump distance, v is the vibration frequency, and E is the migration energy of the defect responsible for diffusion. For the case of purely thermal diffusion, C_{def} is given by

$$C_{\text{def}}^{\text{th}} = \exp(-E_f/kT), \tag{4}$$

where E_f is the formation energy of the defect.

For the case where irradiation enhances diffusion, C_{def} is given by

$$C_{\text{def}} = C_{\text{def}}^{\text{th}} + C_{\text{def}}^{\text{irr}}, \tag{5}$$

where $C_{\text{def}}^{\text{irr}}$ is the steady-state concentration of defects under irradiation, determined by the relative rates of damage and recovery. Thus, the diffusion coefficient associated with an enhancement of the solid-state reaction by irradiation differs from the thermal case only in that the concentration of defects under irradiation is higher.

The third process, called ballistic mixing, is independent of temperature and is given by

$$D_{\text{bal}} = \frac{1}{6} \Gamma a^2, \tag{6}$$

where Γ is the displacement rate (dpa/s) and a is the average distance atoms are displaced in the collision cascade.

Solid-state reaction induced by thermal annealing depends only on the first process, while under irradiation, the three processes are active. We assume here that there is an effective activation energy for migration in the amorphous layer under irradiation, which is a combination of irradiation-enhanced and thermal processes. We can then write

$$D_{\text{eff}}^{\text{am}} = D_{\text{th}}^{\text{am}} + D_{\text{bal}}^{\text{am}} = D_{\text{th}}^{\text{am}} + \frac{1}{6} \Gamma a^2, \tag{7}$$

where $D_{\text{eff}}^{\text{am}}$ is the total effective diffusion coefficient in the amorphous phase under irradiation, $D_{\text{th}}^{\text{am}}$ is the thermal diffusion coefficient in the amorphous layer (enhanced or not by irradiation), and $D_{\text{bal}}^{\text{am}}$ is the ballistic diffusion coefficient.

If the amorphization process is controlled by atomic transport (from a combination of the three processes above) it could occur in the following sequence:

(a) As the irradiation or thermal annealing proceeds, a concentration profile of the mobile element starts to form in the immobile layer. When the Fe concentration at the interface exceeds the critical concentration for amorphization, an amorphous layer forms.

(b) Once the amorphous phase forms, it becomes a barrier for further diffusion and the thickness of the amorphous layer is then proportional to $\sqrt{Dt}$ where D is the diffusion coefficient in the amorphous layer and t is the time.

(c) Once a critical concentration of the mobile element is found at the midpoint of the immobile element layer, that layer is completely amorphized, and the Zr rings disappear.

(d) The remainder of the transformation (consuming the Fe layer) occurs by a gradual increase of Fe concentration in the amorphous layer.

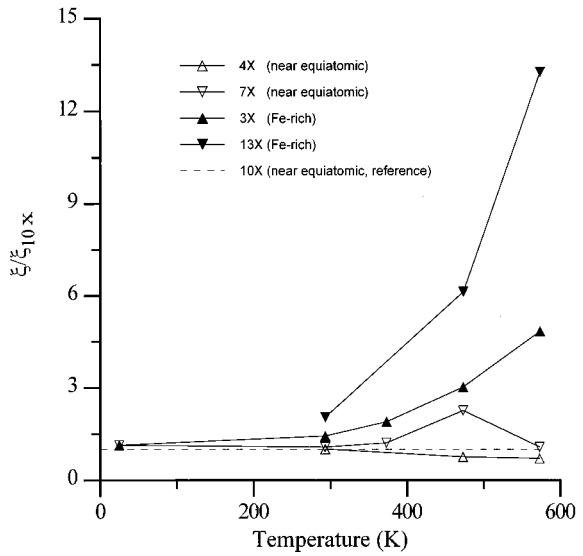

FIG. 12. Amorphization transport ratio ξ for several Zr–Fe multilayers, normalized to the ratio for the 10X multilayer, and plotted against irradiation temperature. The amorphization of the near-equiatomic multilayers is well described by a transport mechanism, but there are significant departures from a pure transport controlled regime for the Fe-rich multilayers.

For an amorphization mechanism controlled by atomic transport, the dose to amorphization is proportional to the square of the multilayer thicknesses, i.e.,

$$\xi = \frac{(\Phi t)_i}{\lambda_i^2} = \frac{(\Phi t)_j}{\lambda_j^2}, \tag{8}$$

where $(\Phi t)_i$ and $(\Phi t)_j$ are the doses to amorphization for multilayers with wavelength λ_i and λ_j. Thus for a transport-controlled mechanism, the ratio $(\xi = (\Phi t)_i/\lambda_i^2)$ should be constant. We plot the ratio ξ/ξ_{10X} in Fig. 12 where the ratio above is normalized to the ratio for the 10X multilayer. The equiatomic multilayers have their ratios close to 1, indicating a transport-controlled mechanism throughout the temperature range. The Fe-rich multilayers increasingly deviate from this behavior at high temperature, indicating more complex processes that could be controlled for example by phase nucleation and interfacial reactions.

Taking the normal error function solution to a diffusion couple problem, the condition for significant diffusion to occur over a length l is

$$l = \sqrt{4 D_{\text{eff}}^{\text{am}} t}. \tag{9}$$

Assuming the Fe is the mobile species, and that amorphization occurs when a critical Fe concentration appears at

TABLE III. Dose to amorphization from Eq. (11) using $a=2.5$ nm.

	Ballistic dose to amorphization [Eq. (11)] (ion.cm^{-2})
4X	7.8×10^{15}
10X	1.2×10^{15}
7X	1.5×10^{15}
3X	7.8×10^{15}
13X	0.38×10^{15}

the middle of the Zr layer, the time to full reaction in a multilayer where the Zr half thickness is $l_{\mathrm{Zr}_{1/2}}$, is given by

$$t_{\mathrm{am}}=\frac{l^2_{\mathrm{Zr}_{1/2}}}{\left[D^{\mathrm{am}}_{\mathrm{th}}+\frac{1}{6}\Gamma a^2\right]}. \tag{10}$$

At low temperature where thermal diffusion is insignificant

$$\Phi t^{\mathrm{bal}}_{\mathrm{am}}=\frac{6l^2_{\mathrm{Zr}_{1/2}}}{a^2\sigma_d}, \tag{11}$$

where $\Gamma=\Phi\sigma_d$, and σ_d is the displacement cross section.

We performed a simple calculation to ascertain whether ballistic mixing alone can explain the results. From a TRIM[12] simulation, the displacement rate is 3×10^{-15} dpa/(Kr ion/cm^2) on the average, and the average size of the displacement cascades of 2–3 nm, so we use 2.5 nm. Using Eq. (11), we calculate the dose to amorphization for each multilayer studied and show the results in Table III.

In Fig. 13 we plot the ratio χ (called the ballistic ratio) of the experimentally measured dose to amorphization (Fig. 5) $(\phi t)_{\mathrm{exp}}$, to the calculated doses to amorphization in Table III $(\Phi t)^{\mathrm{bal}}_{\mathrm{am}}$, which assumes amorphization by a purely ballistic mechanism

$$\chi=\frac{(\Phi t)_{\mathrm{exp}}}{(\Phi t)^{\mathrm{bal}}_{\mathrm{am}}}. \tag{12}$$

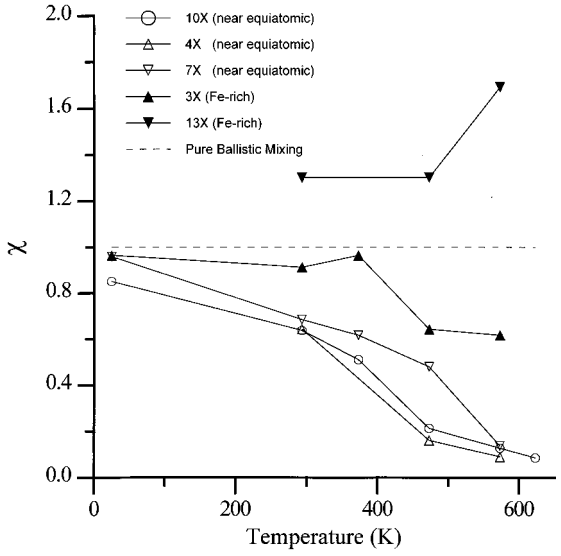

FIG. 13. Ballistic ratio for the amorphization of several Zr–Fe multilayers under Kr ion irradiation plotted against irradiation temperature. Amorphization is well described by a ballistic mechanism at low temperature, but at high temperature there are other processes that also influence amorphization.

If a purely ballistic mechanism were responsible for amorphization, χ would be unity. At low temperature, this appears to be true as χ is close to 1 for both Fe-rich and equiatomic multilayers. This lends support to our initial assumption that Fick's law is approximately valid for these ballistic processes, at least at low temperature. However, as the temperature increases, χ becomes smaller (with the exception of 13X), indicating that a thermally activated process contributes to the reaction. This means that above room temperature the reaction occurs by a combination of ion mixing and radiation enhanced diffusion, such as described by Eq. (4). Kopcewicz and Williamson also observed complete amorphization of equiatomic Zr–Fe multilayers under proton irradiation after a fluence of 2×10^{17} cm^{-2}, nominally at room temperature, and they find that ballistic mixing accounts well for their results.[18] It is not clear why for 13X, χ increases with increasing temperature, but it could be related to the fact that this is the smallest wavelength sample, where the errors in measurement are greatest, and where irregularities in the planar interfaces are comparatively most important.

One unexplained observation is the observation of intermetallic compound formation during irradiation of the 3X, Fe-rich multilayer. The intermetallic compounds observed, Zr_3Fe and $ZrFe_2$, have been previously observed to undergo amorphization during electron and ion irradiation.[46,47] The critical temperature for irradiation induced amorphization of Zr_3Fe under Ar ion irradiation is higher than 500 K.[48] This would lead us to expect that these intermetallic compounds would be unstable under the present irradiation conditions, specially during low temperature irradiations. It is possible that the large compositional gradients that exist in the multilayers under irradiation stabilize the crystalline intermetallic compounds. If that is the case, one would expect that for a high enough dose they would eventually amorphize as the gradients smoothed out.

The thermal annealing results show that as the wavelength increases, crystalline intermetallic compounds are formed in preference to the amorphous phase. Since crystalline intermetallic compounds are the most stable phase, these results are contrary to what would be naturally expected, as the most stable phase is formed more quickly in the sample where the atoms have to travel the greatest distance for mixing. We could resolve this question by invoking the model of Gosele and Tu: in their model, as the wavelength thickness increases, the chemical potential gradients become smaller and it becomes easier to nucleate a crystalline phase from the amorphous phase. The fact that intermetallic compounds form on thick wavelength samples and not on thin wavelength samples is thus consistent with these predictions.[49] Also, the model proposed by Desré and Yavari[50] predicts that the nucleation of crystalline intermetallic compounds

during multilayer reaction is inhibited in the presence of large concentration gradients. This would also tend to favor intermetallic compound formation in the large wavelength samples in preference to the smaller wavelength samples. However, the kinetics do not agree, as the intermetallic phase is formed very fast in the 5X wavelength sample. This issue deserves further investigation.

Finally, the fact that electron irradiation can cause amorphization in these multilayers indicates that intracascade mixing is not necessary for amorphization. This observation is consistent with the hypothesis that the rate-controlling step for amorphization is atomic transport, rather than processes such as direct amorphization in the cascade, or amorphous phase nucleation within the cascade.

V. CONCLUSIONS

Solid-state reactions in Zr–Fe multilayers of various wavelengths and compositions under Kr ion beam irradiation at several temperatures were studied *in situ* using the IVEM/Tandem facility at Argonne National Laboratory. The behavior of the same multilayers under *in situ* thermal annealing was also studied. Observing the reactions in the TEM allowed us to determine the kinetics of the reaction and determine the final products.

(1) For near equiatomic samples, irradiation causes complete amorphization. The dose to amorphization increases in proportion to the square of the wavelength, indicating a diffusion-controlled process. Irradiation with 900 keV electrons at 25 K caused amorphization, showing that displacement cascades are not required for amorphization.

(2) In the equiatomic samples, ion irradiation induced amorphization was athermal below room temperature and occurred faster as the temperature increases toward to 600 K. The activation energy for this second process is 0.17 eV. Above room temperature, diffraction from Zr disappears first indicating that amorphization takes place in the Zr layer by atomic transport of Fe from the Fe layers. These are consistent with a combination of simple ballistic mixing at low temperature and either simple diffusion or radiation enhanced diffusion at higher temperatures.

(3) For the Fe-rich samples, ion irradiation did not cause complete amorphization and crystalline intermetallic compounds Zr_3Fe and $ZrFe_2$ were observed. Amorphization of Fe-rich samples was more sluggish, likely because there was competition with formation of other phases.

(4) Thermal annealing of lower Fe content samples, produced only an amorphous phase and no intermetallic compounds. Thermal annealing of long wavelength, 57% Fe samples resulted in crystalline intermetallic compounds Zr_3Fe and $ZrFe_2$ which became amporhous during subsequent irradiation.

(5) For the equiatomic samples, amorphization doses are consistent with a combination of simple ballistic mixing at low temperature and either simple diffusion or radiation enhanced diffusion at higher temperatures. The behavior of Fe-rich samples could not be described by such simple models, likely due to, the formation of different phases which makes the analysis considerably more complex.

(6) The fact that amorphization occurred more easily in the equiatomic samples than in Fe-rich samples can be explained by a narrow, single minimum, free energy curve for the amorphous phase. This is in agreement with previous experiments by Paesano *et al.*, that suggest that a metastable equilibrium exists between amorphous phase and bcc-Fe at Fe-rich compositions.

ACKNOWLEDGMENTS

The authors would like to thank Ed Ryan for his help in conducting the irradiations and Stan Ockers and Loren Funk of Argonne National Laboratory for their technical assistance. A. Paesano acknowledges a postdoctoral fellowship from the Brazilian National Research Council (CNPq) to work at Penn State. The authors gratefully acknowledge the support of this work by the National Science Foundation (NSF) and by the Brazilian National Research Council, CNPq.

[1] R. B. Schwarz and W. L. Johnson, Phys. Rev. Lett. **51**, 415 (1983).
[2] K. Samwer, Phys. Rep. **161**, 1 (1988).
[3] N. Karpe, J. Bottiger, N. G. Chechenin, and J. P. Krog, Mater. Sci. Eng., A **179/180**, 582 (1994).
[4] H. U. Krebs, D. J. Webb, and A. F. Marshall, Phys. Rev. B **35**, 5392 (1987).
[5] A. Paesano, S. R. Teixeira, and L. Amaral, J. Appl. Phys. **70**, 4870 (1991).
[6] C. Lemaignan and A. T. Motta, in *Nuclear Materials*, edited by B. R. T. Frost (VCH, New York, 1994), Vol. 10B, pp. 1–52.
[7] D. G. Ivey and D. O. Northwood, J. Less-Common Met. **115**, 295 (1986).
[8] K. Yamamoto, T. Nakayama, H. Satoh, T. J. Konno, and R. Sinclair, J. Magn. Magn. Mater. **126**, 128 (1993).
[9] W. Kiauka and W. Keune, Hyperfine Interact. **57**, 1901 (1990).
[10] C. W. Allen and E. A. Ryan, Mater. Res. Soc. Symp. Proc. **439**, 277 (1997).
[11] J. J. Vlassak, T. J. Konno, W. D. Nix, and T. Nakayama, Mater. Res. Soc. Symp. Proc. **239**, 493 (1992).
[12] J. Ziegler, J. P. Biersack, and U. Littmark, *The Stopping and Range of Ions in Matter* (Pergamon Press, New York, 1985).
[13] F. R. Ding, P. R. Okamoto, and L. E. Rehn, J. Mater. Res. **4**, 1444 (1989).
[14] A. T. Motta *et al.*, Nucl. Instrum. Methods. Phys. Res. B (unpublished).
[15] X. W. Lin, D. N. Seidman, and P. R. Okamoto, J. Alloys Compd. **194**, 389 (1993).
[16] D. Arias and J. P. Abriata, Bull. Alloy Phase Diagrams **9**, 597 (1988).
[17] B. M. Clemens and M. J. Suchowski, Appl. Phys. Lett. **47**, 943 (1985).
[18] M. Kopcewicz and D. L. Williamson, J. Appl. Phys. **74**, 4363 (1993).
[19] F. R. Ding, P. R. Okamoto, and L. E. Rehn, Nucl. Instrum. Methods Phys. Res. B **39**, 122 (1989).
[20] N. Karpe, J. Bottiger, J. Janting, and K. Larsen, Philos. Mag. Lett. **63**, 309 (1991).
[21] N. Karpe, J. Bottiger, A. L. Greer, J. Janting, and K. Larsen, J. Mater. Res. **7**, 926 (1992).
[22] W. Kiauka, W. Keune, T. Shinjo, and N. Hosoito, J. Magn. Magn. Mater. **93**, 494 (1991).
[23] W. Kiauka, C. V. Cuyck, and W. Keune, Mater. Sci. Eng., B **12**, 273 (1992).
[24] M. Kopcewicz, J. Jagielski, T. Stobiecki, F. Stobiecki, and G. Gawlik, J. Appl. Phys. **76**, 5232 (1994).
[25] M. Kopecwicz, J. Jagielski, T. Stobiecki, F. Stobiecki, and K. Roll, Mater. Res. Soc. Symp. Proc. **311**, 197 (1993).
[26] H. U. Krebs, D. J. Webb, and A. F. Marshall, J. Less Common Met. Commun. **140**, 17 (1988).
[27] H. U. Krebs, W. Biegel, A. Bienenstock, D. J. Webb, and T. H. Geballe, Mater. Sci. Eng. **97**, 163 (1988).
[28] T. Nakayama, H. Satoh, T. J. Konno, B. M. Clemens, D. A. Stevenson, R. Sinclair, and S. B. Hagstrom, J. Magn. Magn. Mater. **126**, 105 (1993).
[29] T. Nakayama, K. Yamamoto, H. Satoh, T. J. Konno, B. M. Clemens, and R. Sinclair, Mater. Sci. Eng., A **198**, 19 (1995).
[30] T. Otto, T. Stobiecki, F. Stobiecki, and K. Roll, J. Magn. Magn. Mater. **101**, 207 (1991).

[31] A. Paesano, S. R. Teixeira, and L. Amaral, Hyperfine Interact. **67**, 665 (1991).
[32] A. Paesano, A. T. Motta, R. C. Birtcher, E. A. Ryan, S. R. Teixeira, M. E. Bruckmann, and L. Amaral, Mater. Res. Soc. Symp. Proc. **439**, 419 (1997).
[33] D. E. Williamson and B. M. Clemens, Hyperfine Interact. **42**, 967 (1988).
[34] S. Kraegermann, K. Roll, F. Stobiecki, and T. Stobiecki, J. Magn. Magn. Mater. **101**, 209 (1991).
[35] J. Dubowik, F. Stobiecki, H. Rohrmann, and K. Roll, J. Magn. Magn. Mater. **152**, 201 (1996).
[36] C. Michaelsen, M. Piepenbring, and H.-U. Krebs, J. Phys. (France) **51**, 157 (1990).
[37] H. Geisler, U. Herr, T. Lorenz, and K. Samwer, Thin Solid Films **275**, 176 (1996).
[38] K. M. Unruh and C. L. Chien, Phys. Rev. B **30**, 4968 (1984).
[39] C. Hausleitner and J. Hafner, J. Non-Cryst. Solids **144**, 175 (1992).
[40] M. E. Bruckmann, A. Paesano, S. R. Teixeira, and L. Amaral, *International Conference on the Applications of the Mossbauer Effect, Rimini, Italy, 1995*, Italian Physical Society **50**, 627 (1995).
[41] C. Jaouen, A. Michel, J. Pacaud, C. Dufour, Ph. Baure, and B. Gervais, Ion Beam Modification of Materials-98 , (1998).
[42] C. R. Rodriguez, R. H. D. Tendler, L. J. Gallego, and J. A. Alonso, J. Mater. Sci. **30**, 196 (1995).
[43] M. E. Bruckman, A. Paesano, S. R. Teixeira, and L. Amaral, Proceedings of the Latin American Conference on Applications of the Mossbauer Effect, Cuzco, Peru, 1996.
[44] A. T. Motta, J. Nucl. Mater. **244**, 227 (1997).
[45] G. Martin, Phys. Rev. B **30**, 1424 (1984).
[46] A. T. Motta, L. M. Howe, and P. R. Okamoto, J. Nucl. Mater. **205**, 258 (1993).
[47] A. T. Motta, L. M. Howe, and P. R. Okamoto, Mater. Res. Soc. Symp. Proc. **373**, 183 (1995).
[48] L. M. Howe, D. Phillips, A. T. Motta, and P. R. Okamoto, Surf. Coat. Technol. **66**, 411 (1994).
[49] U. Gosele and K. N. Tu, J. Appl. Phys. **53**, 3252 (1982).
[50] P. Desre and A. R. Yavari, Phys. Rev. Lett. **64**, 1533 (1990).